2 Theoretical background

2.1 Ultrashort Laserpulses

The work treats the interaction of few-cycle laser pulses with matter. The basic description of the time evolution of the eletric field of a few-cycle laser pulse is most conveniently described using an envelope $f(t)$ and a phase function ($\phi(t)$). Due to its simplicity often a Gaussian envelope with linear phase is assumed:

$$E(t) = f(t)\cdot\cos(\phi(t)) = \exp(-2\cdot ln(2)(t/\tau)^2)\cdot\cos(\omega_0\cdot t+\phi_{CE}), \quad (2.1)$$

where ω_0 is the central frequency and τ is the intensity-FWHM. The Fourier transform leads to a connection between spectral width and temporal duration for a pulse with flat spectral phase [32]:

$$\tau_p \cdot \Delta\omega = 0.441 \cdot 2\pi. \quad (2.2)$$

where $\Delta\omega$ is the spectral intensity-FWHM. Few-cycle-pulses need an octave-spanning spectrum. As laser pulse described by Eq. 2.1 is plotted in Fig. 2.1. As an be seen for few-cycle laserpulses the CE-phase plays an important role in the time-evolution of the electric field.

J. Schötz, *Attosecond Experiments on Plasmonic Nanostructures*,
BestMasters, DOI 10.1007/978-3-658-13713-7_2

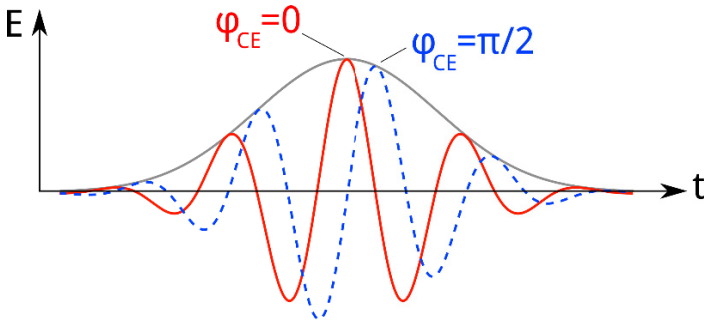

Figure 2.1: A 4.5 fs few-cycle laser pulse centered at 750 nm for two different carrier to envelope phases (ϕ_{CE} or CEP).

2.2 Maxwell's equations

The description of the interaction of electromagnetic fields with macroscopic matter is given in terms of Maxwell's equations [7]:

$$\nabla \cdot \vec{D} = \rho_{ext} \tag{2.3}$$

$$\nabla \cdot \vec{B} = \rho \tag{2.4}$$

$$\nabla \times \vec{E} = -\frac{\partial \vec{B}}{\partial t} \tag{2.5}$$

$$\nabla \times \vec{H} = \vec{J}_{ext} + \frac{\partial \vec{D}}{\partial t} \tag{2.6}$$

where $\vec{E}$ is the electric field, $\vec{D}$ is the electric displacement, $\vec{B}$ the magnetic field and $\vec{H}$ the auxiliary magnetic field and ρ and $\vec{J}$ are the external charge and current densities.

For nonmagnetic media $\vec{D}$ and $\vec{H}$ are linked to the electric and magnetic fields $\vec{E}$ and $\vec{B}$:

$$\vec{D} = \epsilon_0 \vec{E} + \vec{P} = \epsilon_0 \epsilon_r \vec{E} \tag{2.7}$$

$$\vec{B} = \mu_0 \vec{H}, \tag{2.8}$$

where ϵ_r is called the relative permittivity or dielectric function. Due to the interaction of the intrinsic charges and currents within the

medium, the dielectric displacement is dependent on the response of the medium at surrounding positions and earlier times. This can be expressed as a temporal and spatial convolution:

$$\vec{D}(\vec{r},t) = \epsilon_0 \int \mathrm{d}t' \int \mathrm{d}\vec{r}' \epsilon(\vec{r}-\vec{r}', t-t')\vec{E}(\vec{r}', t'). \tag{2.9}$$

By switching to frequency-momentum-space via Fourier transform, we obtain:

$$\vec{E}(\vec{k},\omega) = \epsilon_0 \epsilon_r(\vec{k},\omega)\vec{E}(\vec{k},\omega). \tag{2.10}$$

For electromagnetic radiation the wavelength is usually large compared to the interaction length of the charges in the medium. It is thus save to approximate $\epsilon_r(\vec{k},\omega) = \epsilon_r(\vec{k}=0,\omega) = \epsilon_r(\omega)$, which is equivalent to assuming a local response. We will see in a later chapter, that for the problem of the passage of an electron through matter, the above assumption is not valid and the $\vec{k}$-dependence has to be kept. Generally, the finite response time of the medium, especially for ultrashort pulses, remains important and we have to keep the ω-dependence.

In the description of material properties of metals, the free-electron gas model has been very successful. By considering the polarization response of a free electron to an oscillating electric field $E(t) = E_0 \cdot e^{-i\omega t}$ the so-called Drude dielectric function can be derived:

$$\epsilon_D(\omega) = 1 - \frac{\omega_p^2}{\omega^2 + i\gamma\omega} \tag{2.11}$$

where γ is the damping constant of electron motion. The plasma frequency ω_p is given by:

$$\omega_p = \sqrt{\frac{e^2 \cdot n}{\epsilon_0 m}}, \tag{2.12}$$

where e is the electron charge, n the electron density and m the (effective) mass of an electron. Neglecting the damping, for $\omega = \omega_p$ the dielectric function vanishes and the electric field is given by an

longitudinal depolarization field $\vec{E} = \frac{P}{\epsilon_0}$. This can be interpreted as an collective electron oscillation and is referred to as bulk plasmon [7]. It will play an important role when considering the energy loss of electrons passing through matter.

Mathematically finding the response of a nanoobject to an external field is a boundary value problem. Maxwell's equation lead to the following boundary conditions between medium 1 and medium 2 in the absence of free surface currents:

$$(\vec{E_1} - \vec{E_2}) \times \vec{n} = 0 \tag{2.13}$$

$$(\vec{H_1} - \vec{H_2}) \times \vec{n} = 0 \tag{2.14}$$

where E_1 (H_1) and E_2 (H_2) are the electric (auxiliary magnetic) fields on the left and right of the boundary respectively and $\vec{n}$ is the surface normal. In macroscopic Maxwell equation the surface charge is confined to an infinitesimally thin layer. In realistic materials the interaction of this charges leads to smearing of the surface charge on the length scale of the screening length [6]. The description of this effect requires nonlocal models and is a hot topic in the current research of nanoplasmonics [33, 34].

2.3 Nanoplasmonics

Nanoplasmonics allows overcoming the diffraction limit of light, by coupling collective electron dynamics (plasmons) to the oscillations of the electromagnetic field of light. [8]. Due to the coupling these excitations are called plasmon-polaritons [6]. Within the framework of second quantization of quantum mechanics they can be assigned a quasi-particle character. For classical incoming light (always the case in this thesis) they can however fully be described within the framework of Maxwell's equations [7]. The confinement of light is usually accompanied by enhancement of the electric field near the surface of the plasmonic object. Plasmon-polaritons are distinguished into surface plasmon-polaritons (SPP) and localized surface plasmons (-polaritons, LSP). Surface plasmon-polaritons are electromagnetic

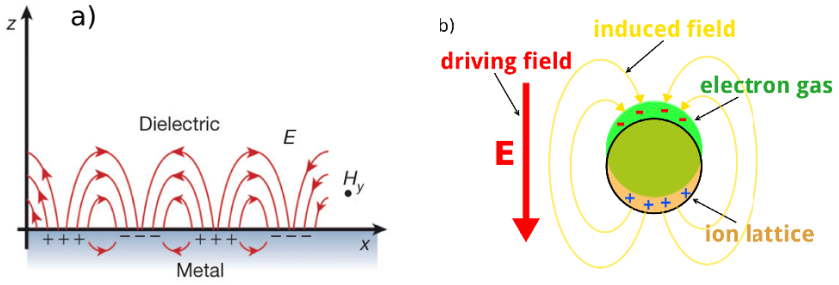

Figure 2.2: a): Illustration of a travelling surface plasmon polariton. The electric field is localized perpendicular to the surface. (from [35]) b): Localized surface plasmon polariton. The driving field causes oscillations of the electrons with respect to the lattice. Superposition of driving field and induced field leads to field enhancement at the poles.

waves which travel along a surface [7] and which are confined to the nanoscale perpendicular to the surface. They are simply solutions of Maxwell's equations coupling quasi-plane waves from both sides of the surface through Eq. 2.13. These solutions can be interpreted as SPPs if they are confined to the surface, which depends on the refractive index of the two media [7]. This is schematically in Fig. 2.2 a). SPPs are not restricted to plane surfaces and occur also on e.g. cylindrical or conical surfaces like the shank of a nanotip [10].

Localized surface plasmons by contrast occur when the dimensions of the particle fall below the wavelength of the incident light. The oscillating electric field of the incoming light causes a collective oscillation of the electrons with respect to the ion lattice [6], which leads to a confinement of optical energy on the order of the geometric features of the nanoobject and to field enhancement. This is schematically shown in Fig. 2.2 b).

2.4 Mie Theory

Mie theory is one of the few examples of an analytic solution to the problem of electromagnetic scattering of a particle in the framework of Maxwell's equations.

An extensive presentation of this subject with a detailed derivation is given in [36]. The basic concept of the solution is actually quite simple and straight-forward, however often obscured by the technical difficulties encountered on the way. We will therefore only outline the general formalism, which is independent of the geometry before briefly sketching the explicit solution for a sphere. The basic formalism starts from the Maxwell equations in a linear homogeneous isotropic medium in frequency-space:

$$\nabla \times \vec{E} = i\omega\mu\vec{H} \tag{2.15}$$

$$\nabla \times \vec{H} = -i\omega\epsilon\vec{E} \tag{2.16}$$

$$\nabla \cdot \vec{E} = 0 \tag{2.17}$$

$$\nabla \cdot \vec{H} = 0. \tag{2.18}$$

From this the well known wave equations can be derived:

$$\Delta\vec{E} + k^2\vec{E} = 0, \tag{2.19}$$

where $k^2 = \omega^2\epsilon\mu$ and analogously for $\vec{H}$. The first decisive step in solving such an equation is by making a general ansatz:

$$\vec{M} = \nabla \times \left(\vec{v}\psi\right) = -\vec{v} \times \left(\nabla\psi\right) \tag{2.20}$$

where $\vec{v}$ is a vector and ψ a scalar function. Plugging this ansatz into the wave-equation leads to

$$\Delta\vec{M} + k^2\vec{M} = \nabla \times \left(\Delta\psi + k^2\psi\right) \tag{2.21}$$

That means for $\vec{M}$ to satisfy the wave-equation, we only have to solve the scalar wave-equation for ψ. So far, we have not said anything about $\vec{v}$. It can be shown, that for Eq. 2.21 to hold, $\vec{v}$ can either be a

(arbitrary) constant vector or the position vector $\vec{r}$ [37]. Moreover we notice that another independent solution to Eq. 2.19 is given by

$$, \vec{N} = \frac{1}{k} \nabla \times \vec{M} \tag{2.22}$$

and that $\nabla \times \vec{N} = k\vec{M}$, using identities for the curl-operator. We can now write the solutions for $\vec{E}$ and $\vec{H}$ in terms of $\vec{M}$ and $\vec{N}$, the electric and auxiliary magnetic fields are linked by 2.15.
$\vec{M}$ and $\vec{N}$ are called vector harmonics and ψ the generating function. The two independent vector harmonics correspond to the two polarizations of light in a homogeneous medium. [37].

In order to solve the actual scattering problem, we first have to solve the scalar wave-equation to obtain a (possibly complete) set of solutions ψ. Then, the general fields inside and outside of the scatterer are expressed through the vector harmonics. Finally, the scattering solution is obtained by imposing the boundary conditions on the parallel components of $\vec{E}$ and $\vec{H}$.

The choice of the coordinate system clearly depends on the symmetry of the problem. Only for three geometries, namely spherical, spheroidal and cylindrical, exact analytic solutions are known [37]. We will briefly sketch the solution for light scattering of a sphere.

The scalar wave equation in a spherical coordinate system reads:

$$\frac{1}{r^2}\frac{\partial}{\partial r}\left(r^2\frac{\partial \psi}{\partial r}\right) + \frac{1}{r^2 \sin\theta}\frac{\partial}{\partial \theta}\left(\sin\theta \frac{\partial \psi}{\partial \theta}\right) + \frac{1}{r^2 \sin\theta}\frac{\partial^2 \psi}{\partial \phi^2} + k^2\psi = 0. \tag{2.23}$$

By making a product ansatz $\psi = R(r)\Theta(\theta)\Phi(\phi)$ we get the set of even (subscript e) and odd (subscript o) solutions:

$$\psi_{emn} = \cos(m\phi) P_n^m(\cos\theta) z_n(kr) \tag{2.24}$$

$$\psi_{omn} = \sin(m\phi) P_n^m(\cos\theta) z_n(kr), \tag{2.25}$$

where P_n^m are the associated Legendre Polynomials, and z_n stands for any pair of the spherical Bessel functions of the first kind j_n, the second kind y_n, or the spherical Hankel functions of the first and

second kind $h_n^{(1)}$ and $h_n^{(2)}$. The set of functions ψ_{emn} and ψ_{omn} forms a complete set. The general electric field can now be written as:

$$\vec{E} = \sum B_{emn}\vec{M}_{emn} + B_{omn}\vec{M}_{omn} + A_{emn}\vec{N}_{emn} + A_{omn}\vec{N}_{omn}. \quad (2.26)$$

The fields outside the sphere a expressed as a sum of incident E_i and scattered field E_s. Using the orthogonality of the vector spherical harmonics, in principle any incident field can be expanded as such a sum. For a plane wave one obtains:

$$E_i = E_0 exp(-ikz) \cdot \vec{e}_x = E_0 exp(-ikr\cos\theta) \cdot \vec{e}_x = \\ = E_0 \sum i^n \frac{2n+1}{n(n+1)} \left(\vec{M}_{o1n}^{(1)} - i\vec{N}_{e1n}^{(1)}\right) \quad (2.27)$$

where the superscript (1) indicates the use of the Bessel function of the first kind. Due to the orthogonality of the vector spherical harmonics we only need to consider the terms $\vec{M_{o1n}}$ and $\vec{N_{e1n}}$ for the scattered fields and the fields inside the sphere. Taking the boundary condition of vanishing scattered fields at infinity, and finite fields at the origin we obtain as ansatz for the field inside the sphere E_1:

$$E_1 = \sum E_n \left(c_n \vec{M}_{o1n}^{(1)} - i d_n \vec{N}_{e1n}^{(1)}\right) \quad (2.28)$$

and for the scattered field E_s:

$$E_s = \sum i a_n \vec{N}_{e1n}^{(3)} - b_n \vec{M}_{o1n}^{(3)}, \quad (2.29)$$

where the superscript (3) denotes the usage of the Hankel function of the first kind. The coefficients a_n, b_n, c_n and d_n now have to be determined by imposing the boundary conditions on $\vec{E}$ and $\vec{H}$ (which follow from 2.15):

$$\left(E_i + E_s - E_1\right) \times \vec{e}_r|_{r=R} = 0 \quad (2.30)$$

$$\left(H_i + H_s - H_1\right) \times \vec{e}_r|_{r=R} = 0. \quad (2.31)$$

Using the size parameter $x = kR$ and the relative refractive index $m = k_1/k$ one obtains the solution:

$$c_n = \frac{\mu_1 j_n(x)[x h_n^{(1)}(x)]' - \mu_1 h_n^{(1)}(x)[x j_n(x)]'}{\mu_1 j_n(x)[x h_n^{(1)}(x)]' - \mu h_n^{(1)}(x)[m x j_n(mx)]'} \tag{2.32}$$

$$d_n = \frac{\mu_1 m j_n(x)[x h_n^{(1)}(x)]' - \mu_1 m h_n^{(1)}(x)[x j_n(x)]'}{\mu m^2 j_n(mx)[x h_n^{(1)}(x)]' - \mu_1 h_n^{(1)}(x)[m x j_n(mx)]'} \tag{2.33}$$

$$a_n = \frac{\mu m^2 j_n(x)[x j_n(x)]' - \mu_1 j_n^{(1)}(x)[m x j_n(mx)]'}{\mu m^2 j_n(mx)[x h_n^{(1)}(x)]' - \mu_1 h_n^{(1)}(x)[m x j_n(mx)]'} \tag{2.34}$$

$$b_n = \frac{\mu_1 j_n(mx)[x j_n(x)]' - \mu j_n^{(1)}(x)[m x j_n(mx)]'}{\mu_1 j_n(mx)[x h_n^{(1)}(x)]' - \mu h_n^{(1)}(x)[m x j_n(mx)]'}. \tag{2.35}$$

The importance of Mie theory in the field of nanoscience is manifold. Besides light scattering, it also allows the description of the plasmon modes and near-fields of a sphere and traveling plasmon modes of a cylinder. The general formalism can be used to obtain for example the fiber modes encountered in Super-Continuum-Generation in hollow-core-fibers (see section 3.1). Last but not least it is often used as a benchmark for computational algorithms.

2.5 Attosecond streaking

2.5.1 Fundamentals of attosecond streaking

The basic principle of attosecond streaking can be understood in a classical picture considering the electron as a point particle. Attosecond streaking is a pump-probe scheme with an XUV attosecond pump pulse and a strong few-cycle IR pump pulse. The XUV pulse leads to photoemission and the emitted electrons are subsequently accelerated by the oscillating field of the IR pulse . This is schematically shown in Fig. 2.3 a). The initial velocity of the electrons depends on the XUV energy which is on the order of 100 eV. In this non-relativistic

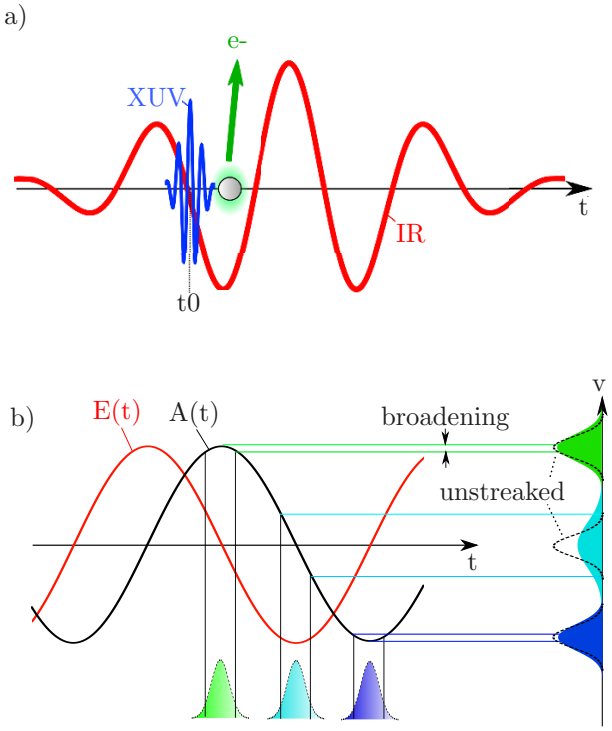

Figure 2.3: Principle of attosecond streaking: a) The time t_0 of electron emission depends on the timing of the XUV attosecond pulse and the few cycle IR pulse. b) The relation between the emission time and the velocity shift experienced by the photoemitted electrons. Features of the XUV pulse are encoded in the change of the shape of the electron spectrum, e.g. the finite temporal duration leads to a delay dependent broadening of the spectrum compared to the unstreaked case (thick dashed line).

regime, omitting the magnetic field, the change of the electron velocity emitted in polarization direction can be written as:

$$\Delta v = -\frac{e}{m}\int_{t_0}^{\infty} \mathrm{d}t\, E(t), \tag{2.36}$$

where it has been assumed that the electric field is homogeneous in space, which is usually a good assumption since the XUV focus is much smaller than the IR focus [38]. Using the relation of the electric field to the vector potential $\frac{\partial \vec{A}}{\partial t} = -E(t)$ and the vanishing DC-component of a laser pulse $\int_{-\infty}^{\infty} E(t) = \mathcal{F}[E(\omega = 0)] = 0 = A(\infty)$, the above equation can be rewritten as:

$$\Delta v = -\frac{e}{m}A(t). \tag{2.37}$$

Depending on the time of emission the electron bunch initiated by the attosecond XUV pulse experiences a velocity shift proportional to the vector potential. This is schematically depicted in Fig 2.3 b).

The final energy is given by

$$\begin{aligned} E(t_0) &= \frac{m}{2}(v_0 + \Delta v)^2 = \\ &= (\hbar\omega - I_p) - \sqrt{\frac{2}{m}(\hbar\omega - I_p)}\frac{e}{m}\cdot A(t_0) + \left(\frac{e}{m}A(t_0)\right)^2, \end{aligned} \tag{2.38}$$

where the last term is usually negligible even for relatively high amplitudes [38]. While the overall shift reflects the vector potential of the IR pulse, the change of the shape of the electron pulse reflects properties of the exciting XUV pulse. In Fig. 2.3 a) this is schematically shown in the delay dependent broadening of the velocity distribution due to the finite temporal duration of the XUV pulse. Also higher order features of the XUV pulse like chirp are encoded in the spectrum and using attosecond streaking both pulses can be characterized [38]. An experimental streaking trace from Neon gas is shown in Fig. 2.4 Attosecond streaking enables to resolve processes on the order of the pulse length of the XUV pulse.

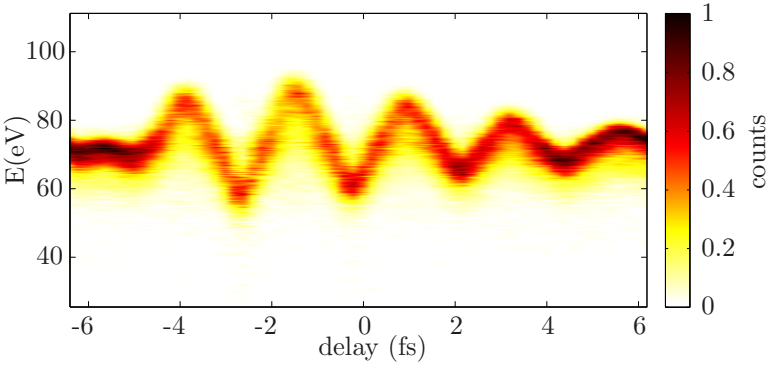

Figure 2.4: An experimental attosecond streaking trace from Neon measured with our setup.

2.5.2 Attosecond streaking from solids

Attosecond streaking has been applied to measure processes on monocrystalline surfaces. Since attosecond streaking is a time-resolved photoemission process, first the theoretical description of photoemission without the IR probe is considered before a brief overview of the existing models of attosecond streaking from solids is given.

Photoemission

Historically one distinguishes between the one-step and three-step picture [39]. The photoemission probability in the one-step pictures and the first step in the three-step picture for weak exciting light fields is given in terms of Fermi's golden rule:

$$P(i \to f) \propto | < \psi_f | \mathcal{H}_{\mathrm{PE}} | \psi_i > |^2 \delta(\hbar\omega - E_f + E_i), \tag{2.39}$$

where ψ_i and ψ_f are the initial and final many-body states respectively, $\hbar\omega$ is the energy of the exciting light. $\mathcal{H}_{\mathcal{PE}}$ is the photoemission operator, which is given by [40]:

$$\mathcal{H}_{\mathcal{PE}} = \frac{ie\hbar}{2m}\left(\nabla \cdot \vec{A} + \vec{A} \cdot \nabla\right) + \frac{e^2}{m}\vec{A}^2, \tag{2.40}$$

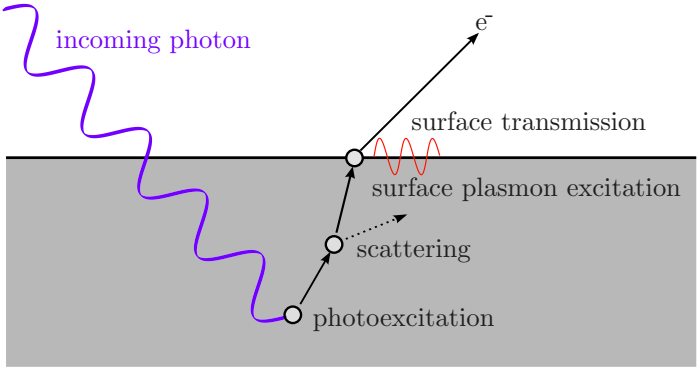

Figure 2.5: The photoemission process in the three step picture.

where $\vec{A}$ is the vector potential.

State-of-the-art models use density functional theory (DFT) to calculate the inital state and are thus able to consistently incorporate the crystal symmetry and effects such as surface reconstruction and recombination [39]. The models differ in the treatment of the final state and electron scattering within the solid. In the one-step model the final state is generally computed by Quantum Field theoretical methods as a state which behaves asymptotically as a free electron and which is scattered inside the solid. It coherently takes into account effects like intrinsic and extrinsic excitations at the price of high computational demand.

In the three-step model, the final state is an eigenstate of the crystal and the computation of Eq. 2.39 leads to the probability of the first step. The three steps are schematically depicted in Fig. 2.5. The second step consists in the transport of the electron to the surface. The probability $P(s)$ that the electron undergoes a scattering event while travelling a distance s, is defined by the material specific mean-free path λ:

$$P(s) \propto e^{-s/\lambda}. \tag{2.41}$$

The inelastic mean free path of most metals for electron energies around 100eV lies in the region of 5 Å [41]. That means that 63%

of the electron suffering no energy loss, are emitted within 5Åfrom the surface. This directly illustrates the surface sensitivity of the photoemission process. The quasiparticle nature of the photoelectron can be accounted for by using an energy dependent group velocity v_G. [42]. The third step is the transmission through the surface, where the electron is transmitted with a probability T and diffracted. Furthermore by passage through the surface, the electron might excite surface plasmons.

The advantage of the three-step model is that it treats different effects such as propagation and transmission as distinct steps, which does not only simplify the description but also allows to describe the the different effects with different degrees of accuracy.

To get a description of attosecond streaking based on this models, the effect of the IR pulse has to be incorporated. In the one-step picture this leads to a different final state, which is again difficult to calculate, whereas in the three-step model it can simply be incorporated into the propagation of the electron.

Attosecond Streaking from Plane Surfaces

The first experiments of attosecond streaking from a plane tungsten surface [22], and subsequent experiments on rhenium [23] and magnesium [24], which focused on measuring time delays between valence and core bands, initiated a number of theoretical models. A recent overview models is given in [33]. All but one [42] use a quantum mechanical description in the single-active electron approximation. The IR-streaking field can either be taken into account by directly solving the time-dependent Schrdinger equation or by employing damped Volkov-states as final states in Eq. 2.39 [33]. Using the symmetry of the experiments, the quasi-perpendicular polarization of XUV and IR with respect to the surface and normal emission, allows a considerable simplification of the models. Different factors such as dispersion or different localization and energy-dependent scattering where used to explain the observed time-shifts of around 100as for tungsten and rhenium and 0 as for magnesium.

Attosecond streaking from nanoplasmonic objets

A number of theoretical studies [25–30] have suggested the use of attosecond streaking for the characterization of nanoplasmonic near-fields. Several points restrict the models for plane surfaces to be used for nanoplasmonics objects. First, due to the changed geometry, the symmetry is reduced, IR and XUV fields are generally not normal to the surface anymore and non-normal electron emission has to be considered. Additionally, the IR fields show pronounced inhomogenities and the considered objects are usually polycristalline. Therefore employed models to describe the attosecond streaking process from nanoobjects are considerably simplified. Electrons are treated in a classical framework. Most models assume electron emission from a narrow band and neglect scattered electrons [25, 27–29] or use an experimental spectrum [26]. Furthermore emission from the surface is assumed and any effects of electron emission and propagation in the solid are neglected, except for [29].

With the first successful attosecond streaking experiments on nanostructures (see Chapter 5), a more detailed model to study the influence of effects neglected above is necessary. Such a model has been developed in this work in the framework of the three-step model. Although the model should be widely applicable, we limit our discussion to attosecond streaking from gold and XUV energies in the region from 80 to 110eV region, the conditions found in experiment. We use a Monte-Carlo algorithm. The XUV beam is described by an Gaussian-profile in space and time and propagates along a straight ray-like line. Over the distances relevant for photoemission the attenuation and the temporal distortion of the XUV-pulse is neglected. This is in agreement with Mie calculations on spheres and cylinders. Since the polarization of the XUV field is numerically hard to calculate and due to the unknown crystal symmetry the photoexcitation is assumed to be isotropic and homogenous and is restricted to a layer a few times the inelastic mean free path from the surface. The initial energy of the electrons is given by the convolution of the experimentally XUV-spectrum and the valence band density of states of gold calculated by

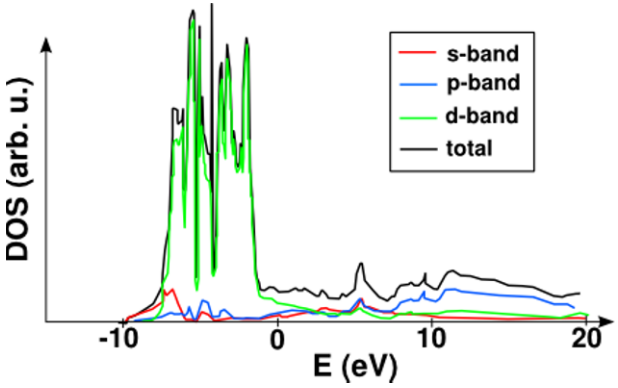

Figure 2.6: partial and total density of states of the valence band of gold calculated by full-potential linear muffin-tin orbital (FP-LMTO) implementation of density-functional theory (DFT) in the local-density approximation (LDA) [43] [adapted from [44]]

density functional theory (DFT) in the full-potential linear muffin-tin implementation (FP-LMTO) using the local density approximation (LDA) [43, 44]. The employed DOS of gold is shown in Fig. 2.6. The electron is subsequently propagated through the medium subject to elastic and inelastic scattering until it reaches the surface, where it is diffracted and may lead to surface excitations. The relation between the DOS and the resulting (unstreaked) photoelectron spectrum is shown in Fig. 2.7. A free electron dispersion is assumed. Scattering and surface transmission are described in great detail in the next chapter. All the time from its birth, the electron is subject to the IR field and the following classical equation of motion is solved numerically:

$$\frac{\mathrm{d}\vec{v}}{\mathrm{d}t} = -\frac{e}{m}\vec{E}_{IR}(\vec{r},t). \tag{2.42}$$

Electron scattering, which changes the electron energy and direction, is assumed to occur instantly. The propagation is stopped when all fields have substantially decayed.

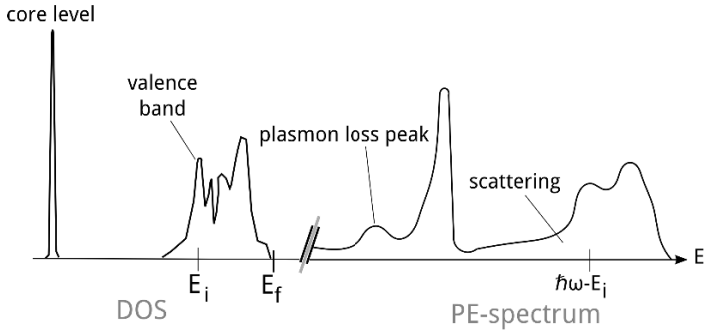

Figure 2.7: Illustration of the relation between the photoemission spectrum and the DOS. The finite width of the exciting photon spectrum as well as scattering lead to a broadening of the features in the photoelectron spectrum.

http://www.springer.com/978-3-658-13712-0

Attosecond Experiments on Plasmonic Nanostructures
Principles and Experiments
Schötz, J.
2016, XIV, 106 p. 45 illus., Softcover
ISBN: 978-3-658-13712-0